

Preparation of single- and double-layer antireflective coatings by sol-gel method

Berrin İkişler

Online Publication Date: 30 July 2019

URL: <http://www.jresm.org/archive/resm2019.105ma0130.html>

DOI: <http://dx.doi.org/10.17515/resm2019.105ma0130>

Journal Abbreviation: *Res. Eng. Struct. Mater.*

To cite this article

İkişler B. Preparation of single- and double-layer antireflective coatings by sol-gel method. *Res. Eng. Struct. Mater.*, 2020; 6(1): 1-21.

Disclaimer

All the opinions and statements expressed in the papers are on the responsibility of author(s) and are not to be regarded as those of the journal of Research on Engineering Structures and Materials (RESM) organization or related parties. The publishers make no warranty, explicit or implied, or make any representation with respect to the contents of any article will be complete or accurate or up to date. The accuracy of any instructions, equations, or other information should be independently verified. The publisher and related parties shall not be liable for any loss, actions, claims, proceedings, demand or costs or damages whatsoever or howsoever caused arising directly or indirectly in connection with use of the information given in the journal or related means.



Published articles are freely available to users under the terms of Creative Commons Attribution - NonCommercial 4.0 International Public License, as currently displayed at [here](https://creativecommons.org/licenses/by-nc/4.0/) (the "CC BY - NC").



Research Article

Preparation of single- and double-layer antireflective coatings by sol-gel method

Berrin İkizler^{*,a}

Department of Chemical Engineering, Ege University, Bornova, İzmir, Turkey

Article Info

Article history:

Received 30 Jan 2019

Revised 19 June 2019

Accepted 28 July 2019

Keywords:

Antireflective glass;

SiO₂;

TiO₂;

Double-layer coating;

Thin films;

Sol-gel method

Abstract

Antireflective (AR) SiO₂ coatings were developed in this work to increase the transmittance of glass in the visible light range of 400-800 nm, due to their potential applications on solar energy systems. Also, double-layer AR coatings were prepared by covering AR SiO₂ layer with a dense TiO₂ layer with the aim of protecting AR layer from environmental effects. SiO₂ coatings were obtained with sol-gel and dip coating methods, by using acid- and base-catalyzed silica sols as precursors. Only 1% transmittance increase was gained with acid-catalyzed SiO₂ coating due to its dense structure. On the contrary, SiO₂ coatings formed by base-catalyzed sol have transmittance > 99% in the 460-660 nm range and of 99.8% at 550 nm, corresponding to the wavelength at maximum intensity of solar spectrum. This high values were attributed to the porous structure of the film revealed by SEM and AFM analysis, and to the optimized thickness of coating achieved at 90-120 mm/min withdrawal speeds. Transmittance of base-catalyzed SiO₂ coatings decreased to an average value of 96.2% after coated with high refractive index TiO₂ layer. However, still a 5-6% achievement in transmittance of glass in 400-800 nm range was attained by optimizing the thickness of each layer using different withdrawal speeds, and concentration and types of the precursor sols. Characterization of the coatings was performed with SEM, AFM, EDS and FTIR analysis.

© 2019 MIM Research Group. All rights reserved.

1. Introduction

Antireflective (AR) coatings decrease the reflectance of the light directed towards them, thus resulting in a high degree of light transmittance. These optical coatings can be applied to all surfaces where a minimum loss of light is required. However, achieving a high transmission of light through glass is an important research subject especially for the solar energy systems, as in photovoltaic and solar thermal devices, to enhance their effectiveness [1-3]. AR coatings are widely applied to increase the solar radiation absorption in these systems, by reducing the natural reflectance loss (~8-9%) of glass components, such as, glass envelopes of the receiver tubes in parabolic trough collectors, glass covers of solar collectors, and glass covers of photovoltaic devices to protect its components from outdoor environment [2-5]. AR coatings are also used in a great number of technological application areas like, high power laser systems, camera and telescope lenses, architectural glasses, eyeglasses, TV screens, display panels, touch screens, etc. [1,6-8].

*Corresponding author: berrin.ikizler@ege.edu.tr

^a orcid.org/0000-0001-8889-0754

DOI: <http://dx.doi.org/10.17515/resm2019.105ma0130>

Res. Eng. Struct. Mat. Vol. 6 Iss. 1 (2020) 1-21

AR coatings attain minimum or zero reflectance if their thickness and also refractive index are appropriately adjusted [8]. The refractive index of an AR coating (n_c) should satisfy the condition given in Eq. (1) to achieve, theoretically, zero-reflectance [8].

$$n_c = (n_0 \times n_s)^{1/2} \quad (1)$$

where n_0 and n_s are the refractive indexes of the medium and the substrate, respectively. Refractive index of glass material, the substrate, is known to be 1.47-1.57. Therefore, AR films applied on a glass surface must have a refractive index (RI) value of 1.21-1.25 to reach zero-reflectivity in air medium ($n_0 \approx 1.0$) [9]. The common materials used as AR coating in the visible range are SiO_2 ($n_c=1.45$), Al_2O_3 ($n_c=1.65$), MgF_2 ($n_c=1.38$), SiO ($n_c=1.85$) and ZnO ($n_c=2.0$) [9,10], but, none of these materials has such a low RI value. Among these materials, SiO_2 is generally preferred due to its relatively low RI value [11]. As the refractive index is proportional to the material density, having a porous structure will help to decrease a material's RI value to the desired levels [11].

Among many coating techniques, it is possible by sol-gel method to produce a porous structure required for achieving a low RI and to control the distribution of the pores within the structure [12]. This method has many advantages when compared to coating technologies such as CVD and sputtering: a simple and inexpensive process; easily coating of even large and complex surfaces, industrial applicability via dipping and spraying; and easy control of process parameters [12-14].

Single-layer AR coatings improve the light transmittance of a substrate effectively but only for narrow wavelength range. For the success in a broad spectrum range, double or multilayer AR coatings are required with an increased optical performance [10,15]. Production of such systems is needed to combine coating layers having different refractive indexes. It is of general practice to choose pairs of materials having high (2.0-2.3) and low (1.45-1.52) indexes [9]. In addition, thickness of each layer should be adjusted in such a way that a destructive interference of light between layers is created, which will consequently cause a low reflectance value. Double-layer AR coatings are generally developed by using a very low refractive index material, such as porous SiO_2 or fluorides, at the outer layer to achieve minimum reflectivity [8,9]. Although these systems attain excellent optical features by this way, their mechanical strength and long-term stability are reported to be relatively poor for outdoor applications [8,9]. Therefore, contrary to the most of the works given in literature [4,9], it is needed to develop double-layer AR systems by covering the inner SiO_2 layer with an outer layer, which will have a protective role against environmental factors [3]. Typically, the materials such as TiO_2 , WO_3 , ZrO_2 , ZnO , SnO_2 and CdS are used for this purpose [3,8,9,16]. Among these, TiO_2 films are distinguished because of its high mechanical strength, high chemical stability and superhydrophilic property under UV light, besides its well-known self-cleaning feature [16]. Nevertheless, its refractive index, 2.3-2.5, is too high [16] so an outer TiO_2 layer will significantly reduce the light transmittance when used in double layer AR systems. Thus, development of multifunctional coatings, integrating the antireflective and durability characteristics into one stack and working in the whole visible light range, are still a challenging task [3]. One of the approaches for this purpose is to make a porous TiO_2 layer over the double layer system to lower its refractive index, and consequently increase the transmittance of the AR system. Removable organic templates (Pluronic F127, Triton X-100, PEG, etc.) are used in the sols as pore making agents, but these methods require high annealing temperatures, like 400-500°C to remove these organic materials [8,12,17]. Another approach is to use colloidal particles dispersed in a solvent [18]. After solvent removal, a porous titania layer is left over the surface. However Zhang et al. [18] found that, the resultant double-layer coating was not too effective to enhance the transmittance of glass. Thus, the goal of the present study is to produce AR double layer coatings

synthesized under very low temperatures with enhanced AR properties that will be applicable to any transparent substrate.

In this work, single-layer SiO₂ and double-layer SiO₂/TiO₂ coatings are developed to maximize the transmission of light through glass slides in the entire visible light range of 400-800 nm. AR features are gained by SiO₂ coatings and TiO₂ is selected to perform as a protective layer. Sol-gel and dip coating techniques are used in the deposition of the coatings. At first step, deposition conditions of single-layer SiO₂ and also single-layer TiO₂ films are optimized individually for a maximum light transmittance. Withdrawal speeds (30-240 mm/min) of the substrates are adjusted for an optimum film thickness of the films. SiO₂ films are obtained using both acid-and base-catalyzed sols in order to change the porosity of the resultant film. However, TiO₂ films are synthesized using only acid-catalyzed sols to form a dense film in the final AR coatings. As a second step, the optimized conditions are combined together to form double-layer SiO₂/TiO₂ coatings. The drawback appeared by the use of TiO₂ as top layer is overcome by controlling the thickness of each layer, so keeping the AR properties of the SiO₂ layer. Coating thickness is optimized by changing the withdrawal speed and concentration of titanium in the coating sol.

2. Materials and Methods

2.1. Materials

All chemicals used in the experiments were of analytical grade and purchased from Sigma-Aldrich. Tetraethyl orthosilicate (TEOS, Si(OC₂H₅)₄, 99%) and tetrabutyl orthotitanate (TBOT, Ti(OC₄H₉)₄, 97%) were used as the precursors of the silica and titania sols, respectively. NH₃ (28-30%) was used as the base catalyst in the system and HCl (37%), as the acid catalyst. Absolute ethanol (EtOH, 99.8%) was selected as the solvent of the sols. Ultrapure water (18.2 MΩ.cm) was used in the experiments and obtained from Millipore Direct-Q8-UV water purification system. Soda-lime glass slides (2.6×7.6 cm, Marienfeld Co.) with thickness of 1 mm were used as substrates for the deposition of coatings. Glass substrates (G, in short) prior to usage were cleaned ultrasonically in acetone and ethanol for 15 min. They were then immersed in concentrated sulfuric acid for one week, followed by thorough washing with distilled water.

2.2. Preparation of Sols

2.2.1 Preparation of SiO₂ Sols

Silica sols were prepared by using either a base or an acid catalyst to investigate the effect of catalyst type on the AR properties. For the base-catalyzed sol, NH₃-EtOH mixture was added dropwise into TEOS-EtOH mixture under vigorous stirring. The resultant sol was stirred further for 2 h at 25°C. The transparent silica sol with a pale blue color was obtained after aging for 2 days at 25°C. The molar ratio of TEOS:H₂O:NH₃:EtOH in the final solution was 1:2.37:1:38 [19], and the concentration of silicon ions was 0.4 mol/L (pH ≈ 10.8). Acid-catalyzed silica sol was prepared by the dropwise addition of H₂O-EtOH mixture into TEOS-HCl-EtOH mixture under vigorous stirring. The molar ratio of TEOS: H₂O:HCl:EtOH in the final solution was 1:4:0.004:80.4 (pH ≈ 3) [20]. The transparent sol was aged for 2 days prior to usage. SiO₂ coatings obtained by using the base-catalyzed sol and by using the acid-catalyzed sol were shortly denoted as B-SiO₂ and A-SiO₂, respectively, in the text.

2.2.2 Preparation of TiO₂ Sols

Titania sols were prepared by hydrolyzing TBOT-HCl-EtOH mixture with the dropwise addition of H₂O-EtOH mixture under vigorous stirring. The resultant transparent acid-catalyzed sol was stirred further for 2 h and also aged for 2 days prior to usage. The molar ratio of TBOT:H₂O:HCl:EtOH was 1:3.55:0.22:164 [20] with a final titanium concentration

of 0.1 mol/L (pH ≈ 1.6). In addition, a titania sol having 0.2 mol/L titanium concentration was also prepared by using the molar ratios of components as 1:3.55:0.22:78.3 (pH ≈ 1.3), to investigate the effect of titanium concentration on the AR properties.

2.3. Deposition of Coatings on Glass Surface

Single-layer SiO₂ (G/SiO₂) or single-layer TiO₂ (G/TiO₂) coatings were obtained by depositing appropriate sols onto the both sides of the clean substrates using dip coating technique. The as-coated films were then dried at 120°C for 3 h in an oven under ambient atmosphere. The effects of dip-coating parameters (withdrawal speed (WS) and also dwell time of the substrates in the sols) were investigated in detail to enhance the AR properties of single-layer coatings.

Double-layer coatings (G/SiO₂/TiO₂) were produced by coating the glass substrates first with SiO₂ layer (inner layer) and then with TiO₂ layer (outer layer). Each layer was heated at 120°C for 3 h. The following parameters were investigated to maximize the AR properties of the double-layer coatings: Withdrawal speeds, catalyst type of the SiO₂ coatings (A-SiO₂ and B-SiO₂) and titanium concentration in the TiO₂ sols (0.1 M and 0.2 M).

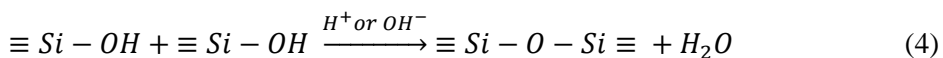
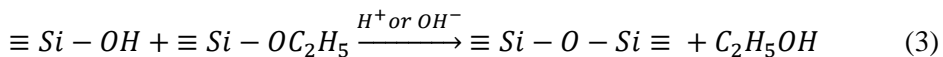
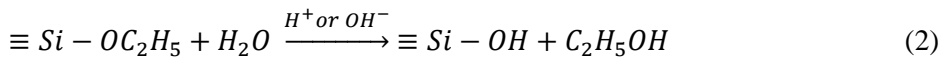
2.4. Characterization

Field emission scanning electron microscopy (SEM, ThermoScientific/Apreo S) was used in the morphological characterization of SiO₂ and TiO₂ coatings. The thickness of the coatings was determined from the cross-sectional SEM view of the samples. The elemental analysis of the coatings in terms of atomic percent was done by energy dispersive X-ray spectroscopy (EDS) connected to the SEM. The surface topography of the coatings was identified by BRUKER-Dimension Edge with ScanAsyst atomic force microscopy (AFM). AFM analysis was conducted in tapping mode for a scan area of 3 μm × 3 μm. The surface roughness values were obtained after the analysis of AFM images and represented in terms of root mean square roughness (R_q). Chemical structure of the films was detected by Fourier transform infrared spectrophotometer (FTIR, Perkin Elmer/Spectra100) with ATR attachment, working in the range of 4000-650 cm⁻¹. AR properties, optical transmittance and reflectance, of the glass substrates before and after coated with different films were determined with UV-Visible spectrophotometer having a 60 mm integrating sphere attachment (Shimadzu/UV-2600-ISR), in the wavelength range of 300-1000 nm.

3. Results and Discussions

3.1. Development of Antireflective SiO₂ Coatings

SiO₂ is used to form an AR layer over glass surface because of its low refractive index (RI) value. SiO₂ film is deposited on the surface with sol-gel polymerization of TEOS in ethanol and water under either acid- or base-catalyzed conditions. A network of Si-O-Si gel is obtained after the hydrolysis of the alkoxy silane, TEOS, as given in Eq. (2) and polycondensation of the hydrolyzed species (Eqs. (3)-(4)) [21].



3.1.1 Effect of Catalyst Type

The hydrolysis and polycondensation reactions, in Eqs. (2)-(4), depend on many parameters like catalyst type, concentration of species, type of solvent, temperature, etc [22]. However, type of catalyst might have the utmost importance in determining the rate of hydrolysis and condensation reactions, thus in turn, the growth behavior of SiO₂ colloidal particles in a gel. Under acid-catalyzed conditions, primary silica particles tend to form linear or randomly branched polymeric chains. These chains entangle and are also cross-linked during growth stage, finally resulting in a dense gel film over the surface [23,24]. The porosity of this dense film is relatively low, therefore, coatings obtained from acid-catalyzed sols have a refractive index value of ~1.44 [23-26], nearly the same as that of bulk SiO₂ ($n_c=1.45$). Using a base catalyst instead leads to a spherically expanding particle (cluster) growth. The growth of these discrete colloidal particles leads to a network structure formation, where voids in nanometer scale are entrapped between them, eventually resulting in a porous film formation over the surface at the end of gelation. Thus, refractive index of SiO₂ coatings obtained by using the base-catalyzed sol (B-SiO₂) is reported to be in the range of 1.12-1.35 depending on the resultant pore volume [19,23,24,27]; remarkable lower than the one using the acid-catalyzed sol (A-SiO₂).

The dense and porous structure of the A-SiO₂ and B-SiO₂ coatings are assessed with SEM analysis, shown in Fig. 1(a) and (b), respectively. The films are coated at 120 mm/min withdrawal speed. Fig. 1(a) points out a smooth and dense surface structure for the acid-catalyzed SiO₂ coatings. This must be the consequence of dense packing of chain-like polymeric particle network. On the contrary, the surface of coatings deposited from the base-catalyzed sol shows a rather rough surface, as given in Fig. 1(b). Silica aggregates (light sides) and voids between them (darker sides) can be distinguished from the top surface view. Similar SEM images were also obtained by Xiao et al. [25] for both acid- and base-catalyzed SiO₂ coatings. The cross-sectional SEM views, given as an inset in Fig. 1(a) and (b), revealed that B-SiO₂ film are formed from individual silica clusters in spherical form while only a dense film is detected in A-SiO₂ coatings, probably because of its small primary particles. The thickness of A-SiO₂ and B-SiO₂ layers is measured as $\sim 31 \pm 3$ nm and $\sim 140 \pm 4$ nm, respectively. The EDS analysis performed during SEM study indicate the existence of only silicon and oxygen atoms in the coatings regardless of the catalyst type. Silicon atom at 33.33 at.% and oxygen atom at 66.67 at.% prove that silica film is in the oxide state, as given in Fig. 1(c) and (d) for A-SiO₂ and B-SiO₂, respectively.

AFM measurements are performed to elucidate more clearly the surface morphologies of SiO₂ coatings and their roughness profiles. The results are shown in Fig. 2 and confirm the SEM observations. Three-dimensional (3D) AFM images verify that acid-catalyzed SiO₂ coating consists of very tiny particles (Fig. 2(a)), whereas, base-catalyzed SiO₂ coating is formed from relatively bigger and discrete particles in spherical form (Fig. 2(b)). The size of particles measured from AFM images, are found to be in the range of 5-20 nm for A-SiO₂ and 30-70 nm for B-SiO₂ coatings, compatible with the mean particle sizes obtained by Vincent et al. [24]. Surface roughness of the coatings is also characterized by AFM analysis for the entire scan area of 3 μ m x 3 μ m. Root mean square roughness (R_q), the standard deviation of the distribution of profile heights, is measured as 0.47 nm for A-SiO₂ and 2.85 nm for B-SiO₂ films. The roughness values of the coatings are in good agreement with the R_q values of acid-catalyzed SiO₂ (0.394 nm) and porous SiO₂ (2.914 nm) coatings, deposited in the work of Wang et al. [28]. The very low R_q value of A-SiO₂ proves that these coatings have atomically smooth surface structure, which could only be obtained by the dense packing of tiny particles. B-SiO₂ film have relatively rough surface when compared to A-SiO₂ film, apparently due to the size of its particles and the voids remained between these discrete particles. Representative cross-sectional views of the 3D images are depicted in Fig. 2(c) and (d) to reveal the height profile changes of the film surfaces

evidently. The height profile (peak heights/valley depths) of A-SiO₂ film remains within the ±1 nm range (Fig. 2(c)), verifying the smoothness of the surface. However, the larger amplitude peaks and valleys within the range of ±6 nm (Fig. 2(d)) for B-SiO₂ film can be attributed to its rough surface structure. Moreover, the peak widths in the surface profiles could be taken as an indication of the size of the particles. When compared to narrow peak widths of A-SiO₂ film, larger peak widths signify the bigger particle existence within the B-SiO₂ film. Smooth and relatively rough surface morphologies for acid- and base-catalyzed SiO₂ coatings were also demonstrated by Li and Shen [26] and Wu et al. [23] in their AFM analysis.

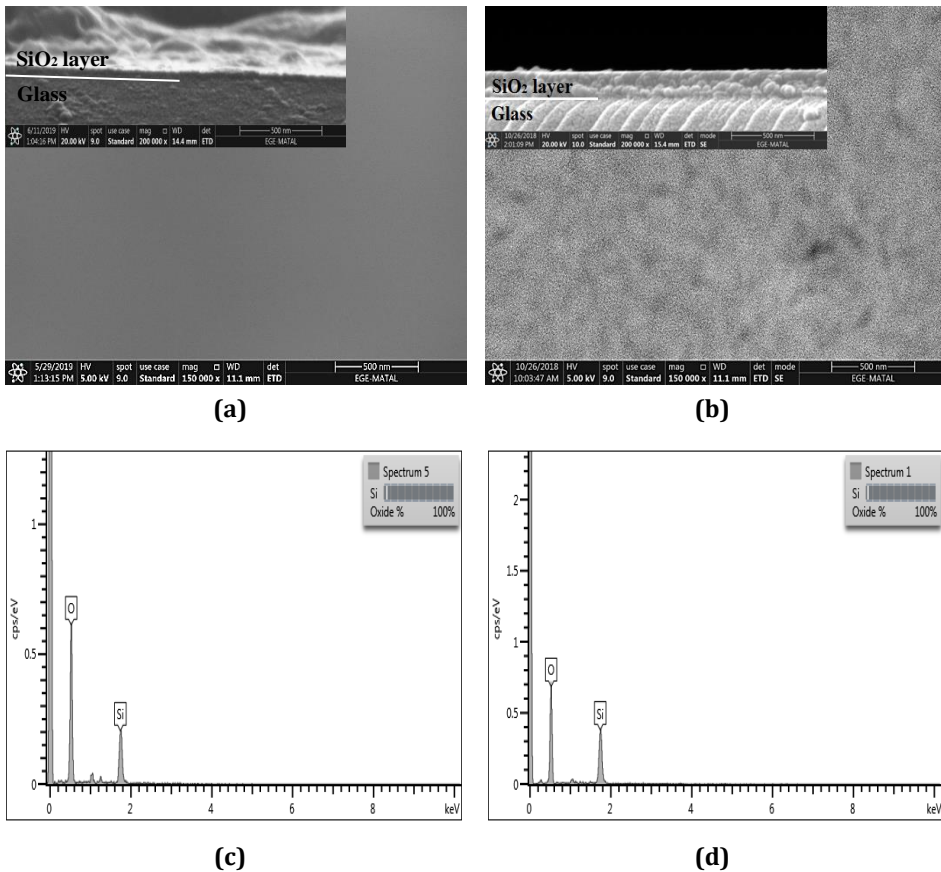


Fig. 1 SEM images of (a) acid-catalyzed and (b) base-catalyzed SiO₂ coatings (The insets show the cross-sectional views); and their corresponding EDS results in (c) and (d), respectively

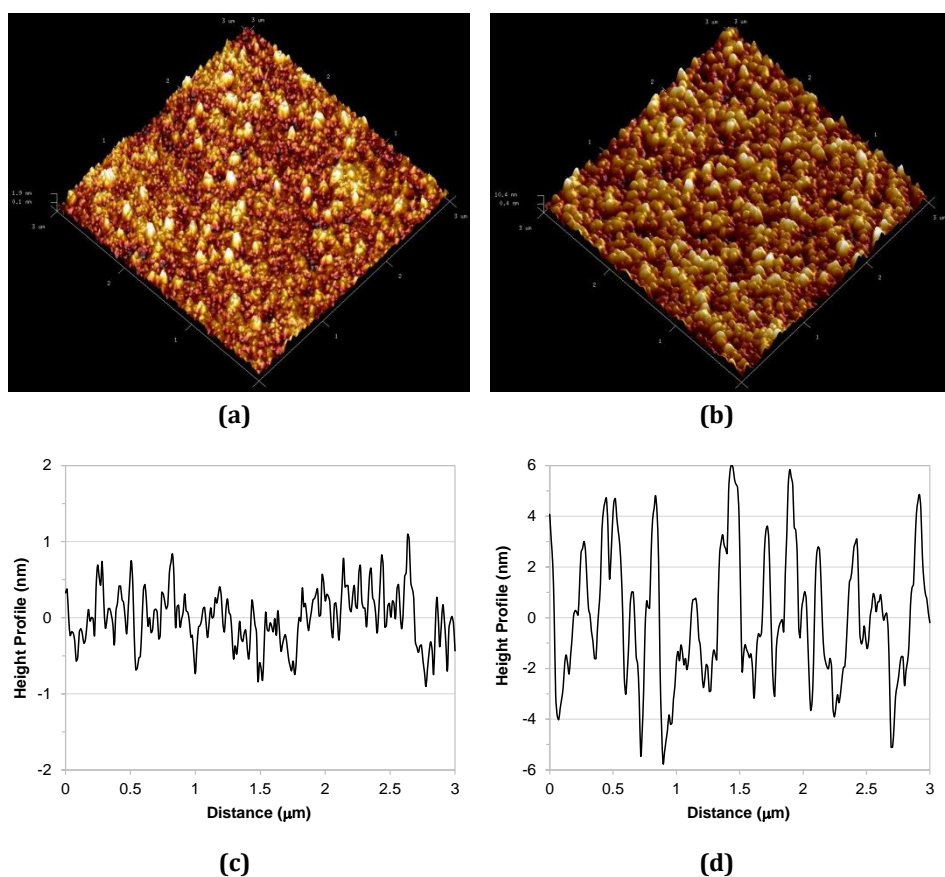


Fig. 2 3D AFM images of (a) acid-catalyzed and (b) base-catalyzed SiO_2 coatings and their cross-sectional scans of the surface profiles in (c) and (d), respectively

Chemical structure of SiO_2 films is confirmed with ATR-FTIR measurements and the results are given in Fig. 3 with the symbols showing the peak locations. Uncoated glass substrate (soda lime silica glass) shows two peaks at $\sim 780\text{-}790\text{ cm}^{-1}$ and $\sim 900\text{ cm}^{-1}$, indicating the symmetric stretching of Si–O–Si bonds and stretching vibrations of Si–OH bonds, respectively [21,29]. Beside peaks coming from the glass substrate, the most intense peak observed at $1060\text{-}1080\text{ cm}^{-1}$ (indicating with an arrow) can be ascribed to the asymmetric stretching of Si–O–Si bonds [21,29]. The presence of this distinct absorption peak verifies the SiO_2 formation over the glass surface for both A- SiO_2 and B- SiO_2 coatings and its network structure, as also indicated by Qian et al. [21] and Ganbavle et al. [30]. Fig. 3 also shows that the intensity ratio of Si–O–Si to Si–OH peaks (at positions 1070 cm^{-1} and 900 cm^{-1}) is higher for B- SiO_2 coatings than A- SiO_2 films, as also found by Vincent et al. [24]. They interpreted this ratio as an indication of the completion of the condensation reaction of silanol group (Si–OH) in SiO_2 films. Therefore it can be deduced that using a base catalyst increases the rate of condensation reaction of silanol group (Si–OH) to form siloxane groups (Si–O–Si) [22-25]. These findings verify that under the acid-catalyzed conditions, hydrolysis is fast and condensation is slow; on the other hand, the condensation rate is faster than hydrolysis rate under the base-catalyzed conditions [22,23,25,31]. Furthermore, the absence of peak at 1400 cm^{-1} (bending of C–H bonds) in B- SiO_2 films implies the purity of the coatings since no residual ethoxy groups exist [19]. However, the

wide weak peak observed at 2985 cm^{-1} (asymmetric stretching of C–H bonds) in addition to the weak peak at 1400 cm^{-1} in A-SiO₂ coatings must be due to the unreacted TEOS precursor [19,30]. All these findings denote that SiO₂ reaction goes to the completion with a base catalyst under low drying temperatures [19].

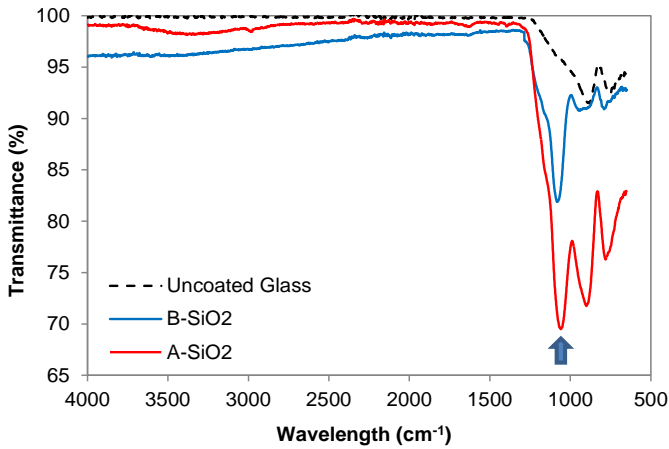


Fig. 3 FTIR spectra of uncoated and SiO₂ coated glass substrates

Optical transmittance (T) and reflectance (R) spectra of SiO₂ coatings obtained using both acid- and base-catalyzed sols are shown in Fig. 4(a) and (b), respectively. Single-layer SiO₂ coatings obviously increase the transmittance of the glass substrates for both catalysts when compared to uncoated one. Average transmittance of uncoated glass, in the whole visible light range of 400-800 nm, is calculated as 91%. Coating the glass surface with base-catalyzed SiO₂ film raises the average transmittance to 98.1% at this wavelength range but with acid-catalyzed SiO₂ film, only to 92.3%. In other words, ~7.1% increase in transmittance is gained with B-SiO₂ coating, compared to ~1.3% increase with A-SiO₂ coating. Substantially higher transmittance of B-SiO₂ film must be the results of its porous structure, as also confirmed by SEM and AFM images. It can be deduced that AR properties of glass is significantly enhanced by B-SiO₂ coatings. Fig. 4(b) also supports this inference. While ~9% of light is reflected from both sides of the air/uncoated glass interface in wavelength range of 400-800 nm, this average value can be reduced to 1.8% by coating the glass surface with B-SiO₂ film. Moreover, it can be lowered to even below 1% in the wavelength range of ~560-790 nm and to a lowest level of 0.4% at 655 nm. However, average reflectance value of glass can only be reduced to 7.7% by A-SiO₂ coating.

Glass substances coated with AR films attain zero-reflectivity in air medium if destructive interference can be created between light reflected from the coating/air interface and coating/glass interface. This condition can only be met if both refractive index and thickness of the applied coating are appropriately chosen [32]: (i). Refractive index value (n_c) of the coatings applied on glass surface should be between 1.21 and 1.25, as can be calculated from Eq. (1). (ii). thickness of coatings (d_c) should be adjusted so that destructive interference can occur at one quarter of the wavelength (λ) of incident light desired [32]:

$$d_c = (\lambda/4)/n_c \tag{5}$$

Reflectivity of base-catalyzed SiO₂ coating could be as low as 0.4% as shown in Fig. 4(b), so it can be inferred that, RI value of these coatings must be within 1.21-1.25 range. RI value of B-SiO₂ coating can be estimated using Eq. (5), considering the wavelength at minimum reflectance ($\lambda = 655\text{ nm}$) in Fig. 4(b) (or maximum transmittance in Fig. 4(a)), and its

coating thickness, $d_c \approx 140$ nm (from Fig. 1(b)). n_c is calculated as ~ 1.17 , in agreement with the experimental n_c results of Xiao et al. [25], Suratwala et al. [19] and also Yan et al. [27] who used approximately the same molar ratio of components with this work. When compared to $n_c = 1.45$ of bulk SiO_2 , this low RI value proves the porous nature of B- SiO_2 coatings. The base-catalyzed hydrolysis leads to bigger particle formation, as determined by AFM images. Void spaces are remained between these bigger particles during particle packing. A porous coating is finally formed at the end of gelation, where air can be entrapped within voids ($n_{air} \approx 1$), resulting in a lower refractive index compound, $n_c \sim 1.17$ [24,33,34]. On the contrary, tiny silica particles are obtained if an acid catalyst is used. When the particle size becomes smaller, void spaces between these particles decrease considerably during the particle packing. Hence, RI of this final dense film is high [24,33]. The reason of the very high transmittance values attained by B- SiO_2 coating compared to dense A- SiO_2 coating must be the lower refractive index of the base-catalyzed film. Therefore, this work is mainly focused on base-catalyzed SiO_2 coatings to achieve zero-reflectivity.

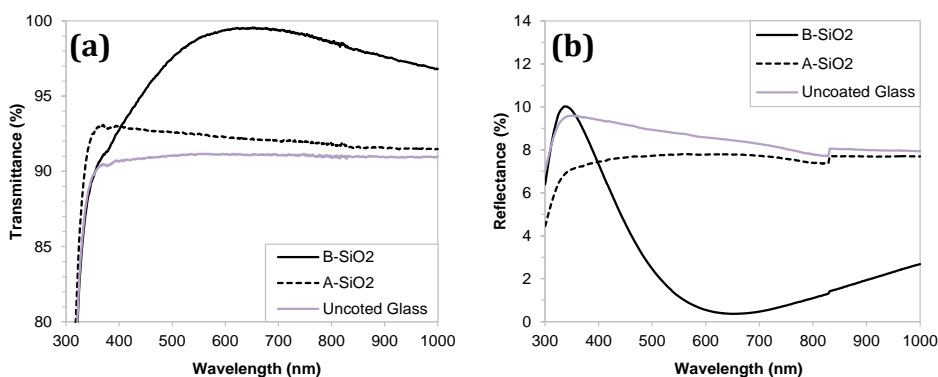


Fig. 4 Effect of catalyst type on (a) transmittance and (b) reflectance spectra of single-layer SiO_2 coatings (WS=120 nm/min)

Surface topography of the coatings must also be taken into consideration to prevent light scattering for attaining zero-reflectivity. A rough surface may lead to optical scattering loss in the transmitted light (transmission haze), especially if the magnitude of the surface roughness is close to the working wavelength of light [3,24,26,35]. Vincent et al. [24] calculated the scattering loss in transmitted light ($T_{diffuse}/T_{total}$ ratio at $\lambda = 550$ nm) caused by the surface roughness of their acid- ($R_q = 0.3$ nm) and base-catalyzed ($R_q = 4.5$ - 16.2 nm) silica films. No any significant surface light scattering was detected in their work and 0.67% maximally, for the base-catalyzed films having $R_q = 16.2$ nm. In addition, using the Rayleigh scattering model (roughness dimensions are lower than the wavelength of light), Mozumder et al. [3] evaluated Rayleigh scattering in the visible region (at $\lambda = 532$ nm) as negligible for silica ($n_c = 1.43$) surfaces if roughness is smaller than 100 nm. Since R_q roughness of both A- SiO_2 ($R_q = 0.5$ nm) and B- SiO_2 ($R_q = 2.9$ nm) coatings in this work is less than 3 nm, it can be inferred that, intensity of the scattering loss in transmitted light can be accepted as negligible in the working wavelength range of $\lambda = 400$ - 800 nm with these very small roughness values of either catalyst type [28,36]. The optical results of this work are the results of total light transmittance (or reflectance) measurements obtained by the integrating sphere attachment. Transmission haze, the percentage ratio of the diffusely (scattered) transmitted light to the total transmitted light ($T_{diffuse}/T_{total}$ or $(T_{total} - T_{direct})/T_{total}$), can be estimated if the intensity of the directly transmitted light values are known [35]. By this approximation, transmission haze is found as 0.4% and 0.9% for A-

SiO₂ and B-SiO₂ coatings, respectively, consistent with the roughness values. In addition, if the thickness of coatings is increased, a maximum haze of 1.1% is observed, showing the high direct transmittance and low transmission haze of the coatings [24,28,35,36].

3.1.2 Effect of Withdrawal Speed

Thickness of coating can be adjusted for minimum reflectivity by changing the withdrawal speed (WS) in the dip coating technique, keeping all other parameters constant. The effect of WS, ranging from 30 to 240 mm/min, on the optical properties of base-catalyzed SiO₂ coatings is shown in Fig. 5. Transmittance spectra in Fig. 5(a) show that B-SiO₂ coatings increase the transmittance of glass for all speeds. However, highest transmittance value (the maximum peak point of the broad spectrum) of 99.8% is reached at WS=90 mm/min. Withdrawal speeds >90 mm/min result in very slight decrease in maximum peak values, from 99.8% to 98.5%. In addition, maximum transmittance peak positions shift towards longer wavelengths with the increase in WS, as noted in Table 1. The red-shift in wavelengths for WS> 90 mm/min can be attributed to an increase in coating thickness, as also detected by Yuan et al. [37] in their working WS range of 48-120 mm/min for porous SiO₂ films and by many others [24,27,29,38]. Considering Eq. (5), this red-shift behavior must be the results of better matching between the refractive index ($n_c \sim 1.17$) and thickness of the coatings, d_c [38]. The theoretical thicknesses are calculated to satisfy the quarter-wave condition at wavelength of maximum transmittance [9,20,38,39]. The d_c results are given in Table 1 and the real film thicknesses measured from the SEM views are in good agreement with these computed d_c values with a maximum difference of 9 nm. The similarity between computed and measured thickness values for AR coatings is also confirmed by Prado et al. [38], Ye et al. [20] and Han and Kim [39]. In addition, it is calculated that coating thickness increases with increasing WS (> 90) according to the relation, $d_c \sim WS^{0.5}$ ($R^2=0.9942$); in accordance with the thickness evolution of the dip-coated films (Theoretically at high withdrawal speeds, viscous drag forces is balanced with gravitational force in the thickness evolution) [17,40]. On the other hand for lower WS (≤ 60 mm/min), the resultant coatings must be too thin and probably more amorphous than the thicker films obtained at WS > 60 mm/min. This might be the reason of relatively lower transmittance values and inconsistency in peak positions at these low speeds. The same trends and findings are also detected in reflectance measurements given in Fig. 5(b). B-SiO₂ coatings significantly decrease the reflectance of glass and minimum reflectance values, changing from 0.3% at 90 mm/min to 0.6% at 240 mm/min, are achieved with a red-shift in the spectra. Hence, it is possible to obtain AR coatings having minimum reflectance at different wavelengths, which will be applicable to different optical end-uses. Effect of WS on acid-catalyzed SiO₂ films was also investigated but only 1.5% gain in transmittance was detected maximally.

Transmittance and reflectance values at 550 nm are drawn in Fig. 5(c) to compare the effectiveness of AR coatings in solar radiation spectrum, since 550 nm wavelength corresponds nearly to the maximum intensity of the solar radiation spectrum [34]. Transmittance increases with the increase in WS up to 90 mm/min, at which maximum transmittance of 99.8% coincides with transmittance at 550 nm wavelength. This value is higher than the transmittance values found in previous reports: e.g. 99% ($\lambda=548$ nm) obtained by Vincent et al. [24] at WS=85 mm/min, 99.4% ($\lambda=500$ nm) achieved by Prado et al. [38] at WS=150 mm/min, 97.5% ($\lambda=500$ nm) found by Mahadik et al. [36] at WS=80 mm/min and 98.78% ($\lambda=550$ nm) found by Xu et al. [34] at WS=162 mm/min. Although the coating parameters are too different in these studies, the coating thicknesses are varied between 100-110 nm. The SEM thickness of B-SiO₂ coating at 90 mm/min is measured as 108 ± 5 nm. Hence, the very high transmittance value attained in this work must be the result of proper adjustment of the required thickness (Table 1) for maximum transmittance at 550 nm based on quarter-wavelength rule. Additionally, the roughness of

the B-SiO₂ coatings is negligibly small to create any scattering loss. With the increase in coating thickness further, WS > 90 mm/min, a nearly linear decrease in transmittance at 550 nm is observed; and it is reduced to 92.7% at 240 mm/min, still higher than that of uncoated glass. Reflectance values show the mirror-image similarity with the transmittance data. A minimum reflectance of ~0.3% is achieved at 90 mm/min and it increases linearly with the increase in WS.

Transmittance values at 550 nm are also compatible with their corresponding average values, calculated in the wavelength range of 400-800 nm and given in Table 1. High average transmittance values of 98.8-94.2% and also low average reflectance values of 1.2-5.1% verify the effectiveness of all B-SiO₂ coatings in the entire visible light range. Nevertheless, the films obtained by WS ≥ 150 mm/min will be more effective at longer wavelengths, as inferred from their higher average transmittance values than their transmittance values at 550 nm. Also, the significant red shift in wavelengths at maximum transmittance for WS ≥ 150 mm/min given in Table 1 substantiates this inference.

Table 1 Transmittance (T) values of single-layer B-SiO₂ coatings deposited at different withdrawal speeds

Coating Name	Withdrawal Speed (mm/min)	Maximum T (%)	Wavelength at Maximum T (nm)	Film Thickness (nm)	Average T at 400-800 nm range (%)
Uncoated Glass (G)	-	-	-	-	91.0
	30	98.2	670	-	96.8
	60	98.7	610	-	98.0
G/B-SiO ₂	90	99.8	550	118	98.8
	120	99.5	655	140	98.1
	150	99.2	720	154	97.0
	180	99.3	790	169	95.9
	200	98.8	820	175	95.1
	240	98.5	890	190	94.2

On the whole, it can be deduced that WS of 90 and also 120 mm/min seem to be the optimum conditions for B-SiO₂ films because of their high transmittance values in terms of both average (98.1-98.8%) and maximum (99.5-99.8%). In terms of average, 7.8% gain at WS = 90 mm/min and 7.1% gain at WS = 120 mm/min shows their effectiveness in the whole visible light range. Furthermore, transmittance of these films is greater than 97% nearly in the entire visible light range and greater than 99% in the broad wavelength range of visible light (460-660 nm at 90 mm/min and 560-760 nm at 120 mm/min). The average transmittance values of 98.8-98.1% at 90-120 mm/min are greater than the average transmittance value of 96.6% at WS = 96mm/min in the work of Yuan et al. [37] corresponding to B-SiO₂ films of the same RI values.

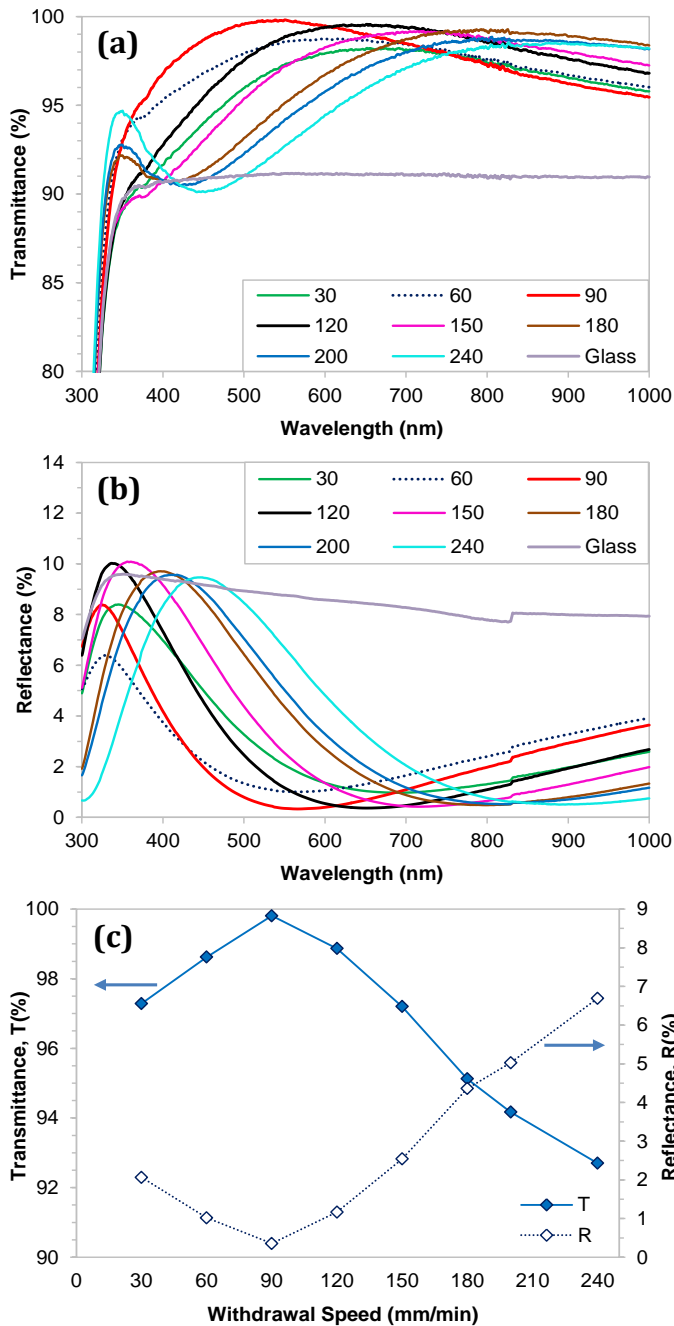


Fig. 5 AR performance of single-layer B-SiO₂ coatings obtained by different withdrawal speeds: (a) transmittance spectra; (b) reflectance spectra; (c) transmittance and reflectance values at 550 nm wavelength

3.2. Development of TiO₂ Coatings

Although base-catalyzed SiO₂ coatings improve the light transmittance of glass considerably, their durability is reported to be quite low because of their porous structure [31]. The connections between spherical particles within the porous film are all point-contacts, thus leading to low durability against scratches and environmental factors [26,31]. Moreover, as the pores get affected by humidity, optical properties of the porous film will get reduced by time [25,26]. Thus, AR coatings also have to possess high durability besides its AR properties for their usage especially in outdoor applications (e.g. solar collectors). In this work, it is aimed to protect porous silica layer from the external factors by coating it with a TiO₂ layer, which have excellent chemical and mechanical durability in addition to well-accepted self-cleaning and superhydrophilic features [32]. The only disadvantage of the TiO₂ film in AR applications is its high refractive index value, $n_c \approx 2.3$ - 2.5 [32,41], since the required condition given in Eq. (1) cannot be not satisfied. Therefore, at first, optimization of the dip-coating process parameters in single-layer TiO₂ film production is performed to maximize the transmittance, before being applied to the multiple coatings.

Transmittance change of TiO₂ films obtained from the sols with different titanium concentrations is shown in Figs. 6(a) with respect to withdrawal speed (Transmittance spectra of TiO₂ coating for WS = 90 and 120 mm/min are given in Fig. 9). TiO₂ film layer reduces the transmittance of glass substrate remarkably below to its uncoated level. Since acid-catalyzed sols are used in TiO₂ deposition, the final dense film must be the reason of low transmittance values. The same results were also found by Miao et al. [41] and they attributed this decline to dense and non-porous film structure of TiO₂. Maximum transmission of light is found at WS = 60-120 mm/min range for all titanium concentrations but the highest at 90 mm/min. Transmittance tends to diminish with further increase in WS (i.e. coating thickness), because of the higher light absorption capacity of the thicker films. An increase in titanium concentration also causes an increase in film thickness [42], so, a further fall in the transmittance of films is detected for [Ti] = 0.2 M sols. Maximum transmittance of 87.4% is achieved at 0.1 M titanium concentration corresponding to a film thickness of 28 ± 4 nm, while it falls to 80.1% at 0.2 M case and even up to 70% at 0.3 M (data not shown here). Parado et al. [38] found transmittance of 41 nm thick dense titania films (WS=150 mm/min) as 79% at 550 nm, by using nearly the same sol composition of [Ti]=0.2 M. Higher titanium concentration of 0.9 M was studied by Touam et al. [43] for three different WS of 10, 20 and 30 mm/min. They obtained only a slight increase with the increase in WS, but transmittance at $\lambda=550$ nm is measured as ~68% for these thick (80-123 nm) titania films. Mohallem et al. [44] investigated the optical transmittance of TiO₂ films for low withdrawal speeds of 12-90 mm/min. The thickness of their films were changed from 40 to 800 nm, depending on the WS, but none of their film achieved to reach over the transmittance of glass (~78% at $\lambda=550$ nm for 40 nm thick TiO₂ films). The results of this work are in good agreement with the previous findings, and transmittance enhancement up to 87.4% is attained by decreasing titanium concentration to 0.1 M and WS to 90 mm/min.

The effect of dwell time at constant WS (120 mm/min) is also investigated, as shown in Fig. 6(b). The substrates are immersed in the sol and allowed for different durations to be completely wetted by the sols before taken out. Extending dwell time does not give much change to the final transmittance of the TiO₂ coatings. However, it is selected as 10 min to ensure that glass surface is uniformly wetted by the sol all over the entire surface.

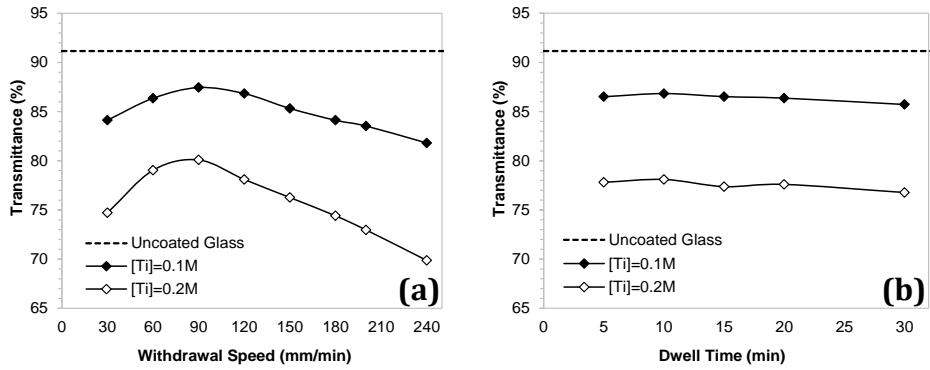


Fig. 6 Transmittance values at 550 nm wavelength of single-layer TiO₂ coatings obtained by different (a) withdrawal speeds, and (b) dwell time

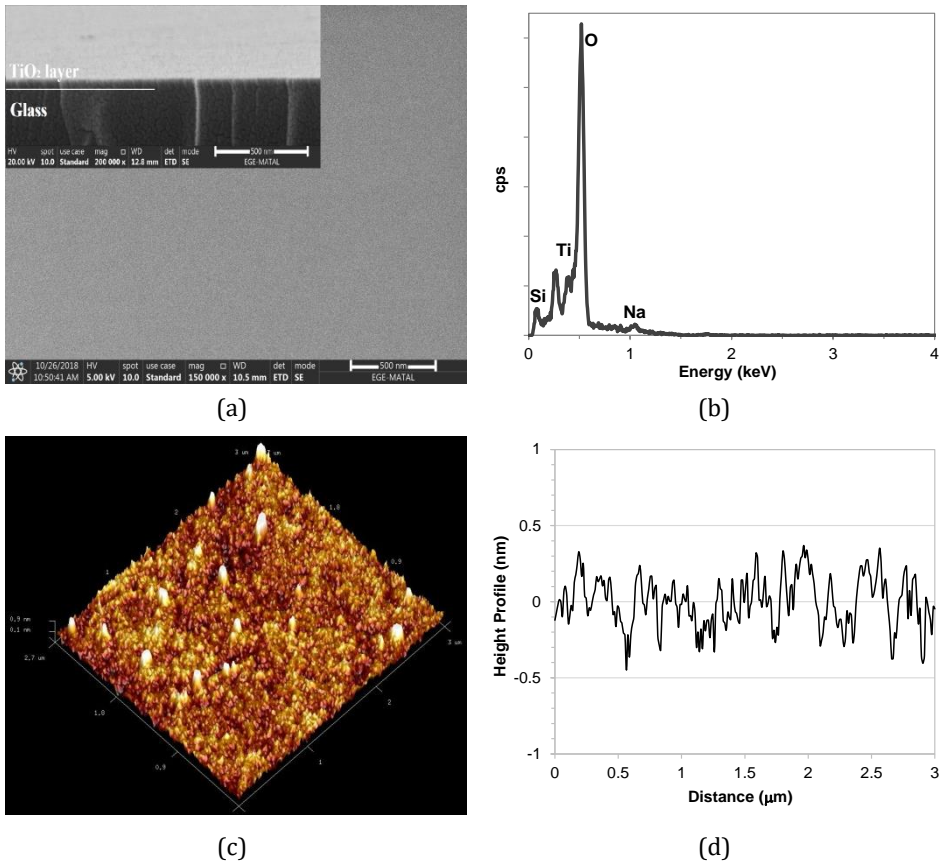


Fig. 7 SEM (a,b) and AFM (c,d) analysis of TiO₂ coatings (WS=120 mm/min): (a) Top view SEM image (inset: cross-sectional view), (b) EDS result, (c) 3D AFM images, (d) AFM cross-sectional scan

SEM view of the TiO₂ coatings, obtained from the sol having 0.1 M titanium concentration, is given in Fig. 7(a). The SEM image verifies a dense, smooth and non-porous film formation over the glass surface. The cross-sectional view of the coatings, represented in Fig. 7(a) as an inset, points out a very thin continuous TiO₂ film formation. The thickness of the film is measured as 34±4 nm for WS=120 mm/min. EDS measurement given in Fig. 7(b) demonstrates the titanium and oxygen existence in the coatings. Since TiO₂ film is too thin, additional peaks (like Si, Na) coming from the glass surface are also detected. FTIR spectra of TiO₂ coatings show the only peaks belonging to the glass substrate, since the characteristic Ti–O bond at around 500-600 cm⁻¹ wavelength range is out of the measurement range (650-4000 cm⁻¹) of the ATR-FTIR (used for film samples) instrument. X-ray diffraction measurements of TiO₂ films are also conducted; however, no peaks could be detected in the XRD pattern. The absence of peaks must be the result of amorphous structure of TiO₂ films. The similar phenomena are also observed in the XRD analysis of the SiO₂ films. Touam et al. [43] for TiO₂ films and also Mahadik et al. [36] for SiO₂ films could not be detected any peaks in their XRD analysis. They attributed the absence of peaks to the amorphous nature of the resultant films.

AFM results confirm the SEM observations. 3D AFM image presented in Fig. 7(c) shows that the surface of the coating is very smooth and covered by tiny particles. The *Rq* roughness of the film is only 0.24 nm, even smaller than the dense A-SiO₂ films, probably due to high acid concentration of titanium sols. A representative line scan of this surface is illustrated in Fig. 7(d). The height profile fluctuations of the coatings changes only within the ±0.5 nm range (Fig. 2(c)), verifying the smoothness of the surface. As the details are given in Section 3.1.1, acid-catalyzed reactions lead to the growth of linearly or randomly branched polymeric particle chains with fast hydrolysis and slow condensation [31,43]. Therefore, the resultant film has a dense structure. These results are in good agreement with several works reported in the literature [20,31,42-44].

3.3. Development of Double-Layer Coatings

Double-layer AR coatings, SiO₂/TiO₂, are produced by coating the antireflective B-SiO₂ layer with TiO₂ layer. The thickness of outer TiO₂ layer is altered by depositing from sols with different titanium concentrations (0.1 M or 0.2 M). Transmittance change of the resultant double-layer coatings at 550 nm wavelength are drawn in Fig. 8 together with their corresponding single-layer coatings. When porous B-SiO₂ film is coated with 34±4 nm thick TiO₂ films, corresponding to 0.1 M titanium sol concentration, transmittance of the resultant stack falls in between to that of single-layer B-SiO₂ and single-layer TiO₂ (0.1 M). Although transmittance of B-SiO₂/TiO₂ (0.1 M) double-layer coatings falls short of the single-layer B-SiO₂ coatings (from 98.9% to 96.3%), B-SiO₂/TiO₂ (0.1 M) system improves the transmittance of glass considerably, ~5% gain. When the thickness of TiO₂ layer is increased to 49±3 nm in B-SiO₂/TiO₂ system by using 0.2 M titanium concentration, transmittance decreases further to 85.8%, which is quite below than that of uncoated glass (91.2%). Lari et al. [45] observed a decline in transmittance of glass to ~89.8% at 550-630 nm range, by coating with SiO₂/porous-TiO₂ double-layer system (WS=25 mm/min) having nearly the same thickness of layers, 150 nm/30 nm, of this work. Miao et al. [41] attained 3.4% gain in transmittance in 400-800 nm range using a porous TiO₂ outer layer in their porous-SiO₂/porous-TiO₂ (48.6 nm/22.5 nm) system. Kesmez et al. [42] also produced SiO₂/TiO₂ coatings with 4-5% gain in transmittance of glass. Hence, ~5% achievement with a dense TiO₂ film can be considered as a good result when compared to previous SiO₂/TiO₂ studies even possessing an outer porous TiO₂ layer. This high gain must be the results of using a very thin TiO₂ layer above the porous SiO₂ layer having very high transmittance [41]. Kesmez et al. [42] emphasized that TiO₂ thickness should be kept as low as possible by decreasing the Ti concentration in order to preserve the AR properties of SiO₂ layer. Furthermore, the results of Ramirez-Garcia et al. [46] showed that outer TiO₂

layer of very small thickness (20-50 nm) still gives improved abrasion resistance and lower transmission haze to the resultant $\text{SiO}_2/\text{TiO}_2$ bilayers. If dense A- SiO_2 film is used in the double-layer system, transmittance of the resultant stack falls to 87.1% by coating with 0.1 M TiO_2 layer and further to 77.1% by coating with 0.2 M TiO_2 layer. It can be deduced that, no any improvement in transmittance of glass could be obtained with A- $\text{SiO}_2/\text{TiO}_2$ double-layer system when nonporous, dense structures are used in both layers. Thus, the introduction of nano pores into the structure seems to be a requisite for higher optical properties.

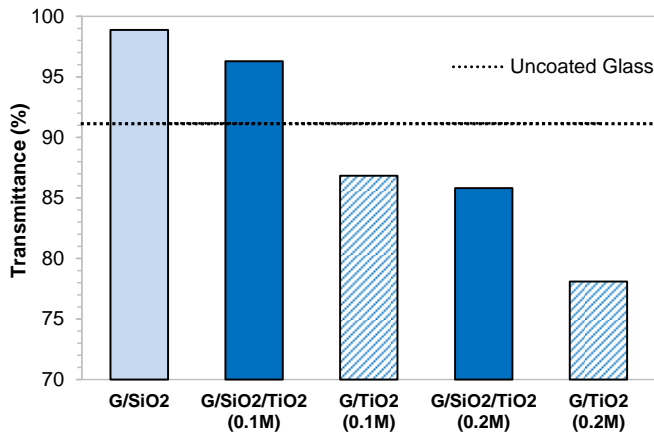


Fig. 8 Transmittance values at 550 nm wavelength of single- and double-layer coatings, obtained by using base-catalyzed SiO_2 film as the inner layer (WS=120 mm/min; the values in parenthesis denote the titanium concentration in TiO_2 sols)

Thickness of each layer in the B- $\text{SiO}_2/\text{TiO}_2$ (0.1M) system is varied by differentiating the withdrawal speeds to investigate any further improvement in transmittance. The results at 550 nm wavelength are given in Table 2. When B- SiO_2 layer is deposited at WS of 90 mm/min ($d_c \approx 108 \pm 5$ nm), as in 90/90 (T=94.3%) and 90/120 (T=93.9%) coatings, transmittance nearly remains constant with the change in TiO_2 film thickness. The single-layer thicknesses of TiO_2 films are 28 ± 4 nm and 34 ± 4 nm for WS = 90 and 120 mm/min, respectively. Nonetheless, when B- SiO_2 layer is coated at 120 mm/min speed ($d_c \approx 140 \pm 4$ nm), highest transmittance of 96.3% is achieved if TiO_2 layer is also coated as thick with 120 mm/min. Another point of view is that, if the outer TiO_2 layer is applied as thick (as in 90/120 and 120/120 coatings), the inner B- SiO_2 layer must be thick also, and vice versa. These results imply that the light waves reflected from the interfaces of the layers interfere destructively mainly in the 120/120 coatings, that is, by the thicknesses of layers obtained at WS=120 mm/min. The thickness of each layer in 120/120 double-layer system is measured using the cross-sectional SEM views, and are found as ~ 138 nm and ~ 37 nm for B- SiO_2 and TiO_2 layers, respectively. The results are compatible with the single-layer thickness measurements. In addition, the existence of silicon and titanium atoms in the double-layer coatings is confirmed with EDX analysis, performed at the same time with SEM measurements.

The AR performance of the B- $\text{SiO}_2/\text{TiO}_2$ double-layer coatings in the whole visible light range (400–800 nm) is evaluated with the transmittance spectra given in Fig. 9, with their corresponding single-layer coatings for comparison. Transmittance of single-layer dense TiO_2 coatings is significantly lower than that of uncoated glass in the entire range. However, the inclusion of an inner B- SiO_2 layer beneath the TiO_2 coatings results in highly effective double-layer coatings. Although their transmittance is not as high as that of

single-layer B-SiO₂ films, AR characteristics of the inner SiO₂ layer are still preserved. B-SiO₂/TiO₂ coated glass, of each layer deposited at 120mm/min, transmits light higher than the uncoated glass in the whole measurement range. Moreover, transmittance $\geq 96\%$ is achieved for wavelengths >530 nm and 98% transmittance is obtained maximally at $\lambda = 750$ nm. When the WS of TiO₂ film is decreased to 90 mm/min, transmittance of 120/90 coatings reaches over to that of uncoated glass after $\lambda > 450$ nm but is still lower than that of 120/120 coatings for all wavelengths. The same phenomena are also observed in 90/90 and 90/120 coatings if thinner B-SiO₂ films of 90 mm/min is used.

Table 2 Transmittance (T) values of single- and double-layer coatings deposited at different withdrawal speeds

Coating Name	Withdrawal Speed, (mm/min)		T at 550 nm, (%)	Average T at 400-800 nm range, (%)
	B-SiO ₂ Layer	TiO ₂ Layer		
G (Uncoated Glass)	-	-	91.2	91.0
G/SiO ₂ /TiO ₂ (90/90)	90	90	94.3	94.4
G/SiO ₂ /TiO ₂ (90/120)	90	120	93.9	94.1
G/SiO ₂ /TiO ₂ (120/90)	120	90	93.8	94.1
G/SiO ₂ /TiO ₂ (120/120)	120	120	96.3	96.2

The average transmittance of coatings at 400–800 nm wavelength range is also calculated and given in Table 2. Average values are in consistency with the values at 550 nm. Table 2 points out that, all double layer coatings bring about an average of 3-5% gain in transmittance to glass slides in the whole visible range. Moreover, in the broad range of wavelength from ~ 500 to 800 nm, an average gain of 6% (or $T \geq 97.2\%$) and 7% gain maximally is achieved with the 120/120 coatings, while an average gain of 4% (or $T \geq 95.1\%$), with all other double-layer coatings. In addition to solar applications [3], transmittance improvement in this wavelength range is also important in the development of high power laser systems [26].

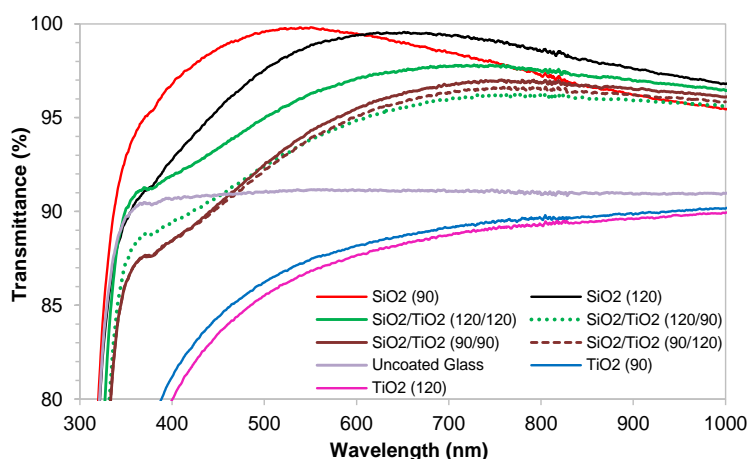


Fig. 9 Transmittance spectra of single- and double-layer coatings (values in parenthesis are the WS of each layer)

4. Conclusion

Single- and double-layer antireflective coatings are developed using sol-gel and dip coating methods to function in the whole visible light range of 400-800 nm. SiO₂ is used as the AR layer and TiO₂ is selected to perform as a protective coating. At first, the optimized conditions in the deposition of single-layer films are determined; then, double-layer coatings of SiO₂/TiO₂ are developed by taking these optimized conditions into account to achieve a high transmittance.

Effect of catalyst type of silica sols (for the porosity change), and also withdrawal speed (for the thickness change) are investigated in the deposition of single-layer SiO₂ films. It is found that, base catalysts gives rise to the formation of a porous B-SiO₂ film, so leading to a decrease in the refractive index value up to ~1.17. Hence, an average of 7-8% gain in transmittance in 400-800 nm range is achieved with B-SiO₂ films when compared to uncoated glass. The results also show that the maximum transmittance of 99.8-99.0% at 550 nm is achieved at 90-120 mm/min speeds corresponding to a coating thickness of ~110-140 nm. Moreover, B-SiO₂ coatings with maximum transmittance working at different wavelengths can be achieved by increasing coating thicknesses further. On the other hand, acid-catalyzed A-SiO₂ coatings have dense structures, resulting in a slight increase in transmittance (only 1-2% gain).

AR coatings have to possess high durability besides their AR properties for the usage in outdoor applications. For this reason, double-layer AR coatings are prepared by covering inner B-SiO₂ layer with an outer TiO₂ film, since the excellent chemical and mechanical durability of TiO₂ is well-accepted in the literature. The inclusion of a nonporous and high RI TiO₂ coating leads to a decrease in transmittance, compared to single-layer B-SiO₂ coatings. However, adjustment of thickness of each layer (to create destructive interference) and the usage of porous SiO₂ film as the inner layer, allow SiO₂/TiO₂ coatings to transmit light higher than the uncoated glass. 5-6% achievement in transmittance of glass, in the whole visible range of 400-800 nm, shows that these coatings can be used in solar energy systems such as glass covers of solar collectors and photovoltaic panels; and also be used in the development of high power laser systems. In addition, these AR coatings can be applied to the all type of transparent surfaces since this production method do not require high temperatures. This work only focuses on the optical properties of double-layer coatings, their durability is under investigation.

Acknowledgements

The author gratefully acknowledges the financial support of Ege University Scientific Research Foundation (Project no: 16-MUH-001).

References

- [1] Huang X, Yuan Y, Liu S, Zhang L, Hong R. Preparation of hydrophobic broadband antireflective SiO₂coating on flexible poly(methyl methacrylate) substrates. *Colloids and Surfaces A: Physicochemical and Engineering Aspects*, 2018; 538: 519 - 525. <https://doi.org/10.1016/j.colsurfa.2017.11.027>
- [2] Agustín-Sáenz C, Machado M, Tercjak A. Antireflective mesoporous silica coatings by optimization of water content in acid-catalyzed sol-gel method for application in glass covers of concentrated photovoltaic modules. *Journal of Colloid and Interface Science*, 2019; 534: 370 - 380. <https://doi.org/10.1016/j.jcis.2018.09.043>
- [3] Mozumder MS, Mourad A-H I, Pervez H, Surkatti R. Recent developments in multifunctional coatings for solar panel applications: A review. *Solar Energy Materials and Solar Cells*, 2019; 189: 75 - 102. <https://doi.org/10.1016/j.solmat.2018.09.015>

- [4] Ye H, Zhang X, Zhang Y, Ye L, Xiao B, Lv H, Jiang B. Preparation of antireflective coatings with high transmittance and enhanced abrasion-resistance by a base/acid two-step catalyzed sol-gel process. *Solar Energy Materials & Solar Cells*, 2011; 95: 2347 - 2351. <https://doi.org/10.1016/j.solmat.2011.04.004>
- [5] Grosjean A, Soum-Glaude A, Neveu P, Thomas L. Comprehensive simulation and optimization of porous SiO₂ antireflective coating to improve glass solar transmittance for solar energy applications. *Solar Energy Materials and Solar Cells*, 2018; 182: 166 - 177. <https://doi.org/10.1016/j.solmat.2018.03.040>
- [6] Xu Y, Liao JX, Cai QW, Yang XX. Preparation of a Highly-Reflective TiO₂/SiO₂/Ag Thin Film with Self-Cleaning Properties by Magnetron Sputtering for Solar Front Reflectors. *Solar Energy Materials & Solar Cells*, 2013; 113: 7 - 12. <https://doi.org/10.1016/j.solmat.2013.01.034>
- [7] Huang WH, Lin CS. Robust superhydrophobic transparent coatings fabricated by a low-temperature sol-gel process. *Applied Surface Science*, 2014; 305: 702 - 709. <https://doi.org/10.1016/j.apsusc.2014.03.179>
- [8] Raut HK, Ganesh VA, Nair AS, Ramakrishna S. Anti-reflective coatings: A critical, in-depth review. *Energy Environ. Sci.*, 2011; 4: 3779 - 3804. <https://doi.org/10.1039/c1ee01297e>
- [9] Priyadarshini BG, Sharma AK. Design of multi-layer anti-reflection coating for terrestrial solar panel glass. *Bull. Mater. Sci.*, 2016; 39(3): 683 - 689. <https://doi.org/10.1007/s12034-016-1195-x>
- [10] Kavaklı İ.G., Kantarlı K. Single and Double-Layer Antireflection Coatings on Silicon. *Turkish Journal of Physics*, 2002; 26: 349 - 354.
- [11] Biswas PK, Sujatha Devi P, Chakraborty PK, Chatterjee A, Ganguli D. Porous Anti-Reflective Silica Coatings with a High Spectral Coverage by Sol-Gel Spin Coating Technique. *Journal of Materials Science Letters*, 2003; 22: 181 - 183. <https://doi.org/10.1023/A:1022241707860>
- [12] Atkinson C, Sansom CL, Almond HJ, Shaw CP. Coatings for concentrating solar systems - A review. *Renewable and Sustainable Energy Reviews*, 2015; 45: 113 - 122. <https://doi.org/10.1016/j.rser.2015.01.015>
- [13] Nagamedianova Z, Ramirez-Garcia RE, Flores-Arevalo SV, Miki-Yoshida M, Arroyo-Ortega M. Solar heat reflective glass by nanostructured sol-gel multilayer coatings. *Optical Materials*, 2011; 33: 1999 - 2005. <https://doi.org/10.1016/j.optmat.2011.04.006>
- [14] Vicente GS, Bayon R, German N, Morales A. Long-term durability of sol-gel porous coatings for solar glass covers. *Thin Solid Films*, 2009; 517: 3157 - 3160. <https://doi.org/10.1016/j.tsf.2008.11.079>
- [15] Chen D, Yan Y, Westenberg E, Niebauer E, Sakaitani N, Chaudhuri SR. Development of Anti-Reflection (AR) Coating on Plastic Panels for Display Applications. *Journal of Sol-Gel Science and Technology*, 2000; 19: 77 - 82. <https://doi.org/10.1023/A:1008714205813>
- [16] Ennaceri H, Erfurt D, Wang L, Köhler T, Taleb A, Khaldoun A, El Kenz A, Benyoussef A, Ennaoui A. Deposition of multifunctional TiO₂ and ZnO top-protective coatings for CSP application. *Surface & Coatings Technology*, 2016; 298: 103 - 113. <https://doi.org/10.1016/j.surfcoat.2016.04.048>
- [17] Zhang W, Tu J, Long W, Lai W, Sheng Y, Guo T. Preparation of SiO₂ anti-reflection coatings by sol-gel method. *Energy Procedia*, 2017; 130: 72 - 76. <https://doi.org/10.1016/j.egypro.2017.09.398>
- [18] Zhang H, Fan D-W, Yu T-Z, Wang C-L. Antireflective and Self-cleaning Properties of SiO₂/TiO₂ Double-Layer Films Prepared by Cost-Effective Sol-Gel Process. *Chinese Journal of Chemical Physics*, 2015; 28: 777 - 780. <https://doi.org/10.1063/1674-0068/28/cjcp1504074>

- [19] Suratwala TI, Hanna ML, Miller EL, Whitman PK, Thomas IM, Ehrmann PR, Maxwell RS, Burnham AK. Surface chemistry and trimethylsilyl functionalization of Stöber silica sols. *Journal of Non-Crystalline Solids*, 2003; 316: 349 - 363. [https://doi.org/10.1016/S0022-3093\(02\)01629-0](https://doi.org/10.1016/S0022-3093(02)01629-0)
- [20] Ye L, Zhang Y, Zhang X, Hu T, Ji R, Ding B, Jiang B. Sol-gel preparation of SiO₂/TiO₂/SiO₂-TiO₂ broadband antireflective coating for solar cell cover glass. *Solar Energy Materials & Solar Cells*, 2013; 111: 160 - 164. <https://doi.org/10.1016/j.solmat.2012.12.037>
- [21] Qian Z, Wang S, Ye X, Liu Z, Wu Z. Corrosion resistance and wetting properties of silica-based superhydrophobic coatings on AZ31B Mg alloy surfaces. *Applied Surface Science*, 2018; 453: 1 - 10. <https://doi.org/10.1016/j.apsusc.2018.05.086>
- [22] Thomas IM. Methods for the preparation of porous silica antireflection coatings varying in refractive index from 1.22 to 1.44. *Applied Optics*, 1992; 31(28): 6145 - 6149. <https://doi.org/10.1364/AO.31.006145>
- [23] Wu G, Wang J, Shen J, Yang T, Zhang Q, Zhou B, Deng Z, Fan B, Zhou D, Zhang F. A novel route to control refractive index of sol-gel derived nano-porous silica films used as broadband antireflective coatings. *Materials Science and Engineering*, 2000; B78: 135 - 139. [https://doi.org/10.1016/S0921-5107\(00\)00529-8](https://doi.org/10.1016/S0921-5107(00)00529-8)
- [24] Vincent A, Babu S, Brinley E, Karakoti A, Deshpande S, Seal S. Role of catalyst on refractive index tunability of porous silica antireflective coatings by sol-gel technique. *Journal of Physical Chemistry C*, 2007; 111: 8291 - 8298. <https://doi.org/10.1021/jp0700736>
- [25] Xiao Y, Shen J, Xie Z, Zhou B, Wu G. Microstructure Control of Nanoporous Silica Thin Film Prepared by Sol-Gel Process. *J. Mater. Sci. Technol.*, 2007; 23(4): 504 - 508.
- [26] Li X, Shen J. A scratch-resistant and hydrophobic broadband antireflective coating by sol-gel method. *Thin Solid Films*, 2011; 519: 6236 - 6240. <https://doi.org/10.1016/j.tsf.2011.03.114>
- [27] Yan G, Yuan Y, Hong R. Preparation of broadband antireflective coatings with ultra-low refractive index layer by sol-gel method. *Construction and Building Materials*, 2018; 176: 75 - 80. <https://doi.org/10.1016/j.conbuildmat.2018.05.016>
- [28] Wang J, Yang C, Liu Y, Zhang C, Zhang C, Wang M, Zhang J, Cui X, Ding R, Xu Y. Broadband antireflective double-layer mesoporous silica coating with strong abrasion-resistance for solar cell glass. *RSC Adv.*, 2016; 6: 25191 - 25197. <https://doi.org/10.1039/C6RA02281B>
- [29] Nielsen KH, Orzol DK, Koynov S, Carney S. Large area, low cost anti-reflective coating for solar glasses. *Solar Energy Materials & Solar Cells*, 2014; 128: 283 - 288. <https://doi.org/10.1016/j.solmat.2014.05.034>
- [30] Ganbavle VV, Bangi UKH, Latthe SS, Mahadik SA, Rao AV. Self-cleaning Silica Coatings on Glass by Single Step Sol-gel Route. *Surface & Coatings Technology*, 2011; 205: 5338 - 5344. <https://doi.org/10.1016/j.surfcoat.2011.05.055>
- [31] Wang X, Shen J. Sol-gel derived durable antireflective coating for solar glass. *Journal of Sol-Gel Sci. Technology*, 2010; 53: 322 - 327. <https://doi.org/10.1007/s10971-009-2095-y>
- [32] Yao L, He J. Recent progress in antireflection and self-cleaning technology - From surface engineering to functional surfaces. *Progress in Materials Science*, 2014; 61: 94 - 143. <https://doi.org/10.1016/j.pmatsci.2013.12.003>
- [33] Choi J, Han K, Kim JK. Enhanced Near Infrared Reflectance of TiO₂/SiO₂/TiO₂ Multilayer Structure Using a Base-catalyzed SiO₂ Film. *Thin Solid Films*, 2014; 569: 100 - 103. <https://doi.org/10.1016/j.tsf.2014.08.036>
- [34] Xu J, Liu Y, Du W, Lei W, Si X, Zhou T, Lin J, Peng L. Superhydrophobic silica antireflective coatings with high transmittance via one-step sol-gel process. *Thin Solid Films*, 2017; 631: 193 - 199. <https://doi.org/10.1016/j.tsf.2017.03.005>

- [35] Zhao L, Strobach E, Bhatia B, Yang S, Leroy A, Zhang L, Wang AN. Theoretical and experimental investigation of haze in transparent aerogels. *Optics Express*, 2019; 27: A39 - A50. <https://doi.org/10.1364/OE.27.000A39>
- [36] Mahadik DB, Lakshmi RV, Barshilia HC. High performance single layer nano-porous antireflection coatings on glass by sol-gel process for solar energy applications. *Solar Energy Materials & Solar Cells*, 2015; 140: 61 - 68. <https://doi.org/10.1016/j.solmat.2015.03.023>
- [37] Yuan Y, Lu X, Yan G, Hong R. Sol-gel preparation of antireflective coatings with abrasion resistance by base/acid double catalysis and surface treatment. *Solar Energy*, 2017; 155: 1366 - 1372. <https://doi.org/10.1016/j.solener.2017.08.003>
- [38] Prado R, Beobide G, Marcaide A, Goikoetxea J, Aranzabe A. Development of Multifunctional Sol-Gel Coatings: Anti-reflection Coatings with Enhanced Self-Cleaning Capacity. *Solar Energy Materials & Solar Cells*, 2010; 94: 1081 - 1088. <https://doi.org/10.1016/j.solmat.2010.02.031>
- [39] Han K, Kim JH. Reflectance modulation of transparent multilayer thin films for energy efficient window applications. *Materials Letters*, 2011; 65: 2466 - 2469. <https://doi.org/10.1016/j.matlet.2011.05.006>
- [40] Hwang J, Shoji N, Endo A, Daiguji H. Effect of Withdrawal Speed on Film Thickness and Hexagonal Pore-Array Dimensions of SBA-15 Mesoporous Silica Thin Film. *Langmuir*, 2014; 30: 15550 - 15559. <https://doi.org/10.1021/la5037713>
- [41] Miao L, Su LF, Tanemura S, Fisher CAJ, Zhao LL, Liang Q, Xu G. Cost-effective nanoporous SiO₂-TiO₂ coating on glass substrates with antireflective and self-cleaning properties. *Applied Energy*, 2013; 112: 1198 - 1205. <https://doi.org/10.1016/j.apenergy.2013.03.043>
- [42] Kesmez Ö, Çamurlu HE, Burunkaya E, Arpaç E. Sol-gel preparation and characterization of anti-reflective and self-cleaning SiO₂-TiO₂ double-layer nanometric films. *Solar Energy Materials & Solar Cells*, 2009; 93: 1833 - 1839. <https://doi.org/10.1016/j.solmat.2009.06.022>
- [43] Touam T, Atoui M, Hadjoub I, Chelouche A, Boudine B, Fischer A, Boudrioua A, Doghmane A. Effects of dip-coating speed and annealing temperature on structural, morphological and optical properties of sol-gel nano-structured TiO₂ thin films. *The European Physical Journal of Applied Physics*, 2014; 67: 30302. <https://doi.org/10.1051/epjap/2014140228>
- [44] Mohallem NDS, Viana MM, Lopes de Jesus MA, Moraes, Gomes GHM, Lima LFS, Alves EDL. Pure and Nanocomposite Thin Films Based on TiO₂ Prepared by Sol-Gel Process: Characterization and Applications, Titanium Dioxide- Material for a Sustainable Environment, Edt. Dongfang Yang, IntechOpen, 2018. <https://doi.org/10.5772/intechopen.74335>
- [45] Lari N, Ahangarani S, Shanaghi A. Effect of Different TiO₂-SiO₂ Multilayer Coatings Applied by Sol-Gel Method on Antireflective Property. *Journal of Materials Engineering and Performance*, 2015; 24: 2645 - 2652. <https://doi.org/10.1007/s11665-015-1547-5>
- [46] Ramírez-García RE, Perez-Garcia SAA, Gonzalez-Rodriguez JA, Arroyo-Ortega M, Licea-Jimenez L. Engineered TiO₂ and SiO₂-TiO₂ Films on Silica Coated Glass for Increased Thin Film Durability Under Abrasive Conditions. *International Journal of Applied Ceramic Technology*, 2017; 14: 39-49. <https://doi.org/10.1111/ijac.12614>